PHOTONICS Research

Analysis of TM/TE mode enhancement and droop reduction by a nanoporous n-AlGaN underlayer in a 290 nm UV-LED

Yufeng Li,[1] Chenyu Wang,[1] Ye Zhang,[1,2] Peng Hu,[1] Shengnan Zhang,[2] Mengqi Du,[2] Xilin Su,[2] Qiang Li,[2] and Feng Yun[1,2,*]

[1]Shaanxi Provincial Key Laboratory of Photonics & Information Technology, Xi'an Jiaotong University, Xi'an 710049, China
[2]Solid-State Lighting Engineering Research Center, Xi'an Jiaotong University, Xi'an 710049, China
*Corresponding author: fyun2010@mail.xjtu.edu.cn

Received 13 January 2020; revised 13 March 2020; accepted 18 March 2020; posted 20 March 2020 (Doc. ID 387607); published 6 May 2020

A full structure 290-nm ultraviolet light-emitting diode (UV-LED) with a nanoporous n-AlGaN underlayer was fabricated by top via hole formation followed by high-voltage electrochemical etching. The 20 to 120 nm nanopores were prepared in regular doped n-AlGaN by adjusting the etching voltage. The comparison between the Raman spectrum and the photoluminescence wavelength shows that the biaxial stress in the nanoporous material is obviously relaxed. The photoluminescence enhancement was found to be highly dependent on the size of the pores. It not only improves the extraction efficiency of top-emitting transverse-electric (TE)-mode photons but also greatly improves the efficiency of side-emitting transverse-magnetic (TM)-mode photons. This leads to the polarization change of the side-emitting light from −0.08 to −0.242. The intensity of the electroluminescence was increased by 36.5% at 100 mA, and the efficiency droop at high current was found to decrease from 61% to 31%.

https://doi.org/10.1364/PRJ.387607

1. INTRODUCTION

The semiconductor-based ultra-violet (UV) light source has great potential to replace the traditional bulky mercury lamp. It is widely used in sterilization, purification, bioanalytics, medical applications, chemical sensing, curing, fluorescence analysis, and so on [1]. Despite great advances in the development of AlGaN-based UV light-emitting diodes (LEDs), the AlGaN-based ultraviolet radiation c (UVC) LEDs are still held back from commercial applications due to their poor external quantum efficiency (EQE). The largest EQE for an encapsulated 270–280 nm UVC LED reported so far is only slightly over 20% [2], and the EQE for most of the bare UVC LED dies is below 10% [3]. This falls far behind visible LEDs based on GaN/InGaN (peak EQE value of 80% for blue, 44% for green, and 63% for red) [4]. Material quality and epitaxial structure design are two of the main challenges. Some remarkable developments include the thin electron-blocking layer (EBL) [5], the sputtered and high-temperature annealed AlN/sapphire template [6], the patterned Si(111) substrate [7], and the low threading-dislocation density (TDD) AlN buffer, which produces high internal quantum efficiency (IQE) of more than 60% [8]. On the other hand, the light extraction efficiency (LEE) remains a big challenge that needs to be solved with great effort. Previous studies have shown that the predominant optical polarization switched from transverse-electric [TE, $(E \perp c)$] mode to transverse-magnetic [TM $(E \parallel c)$] mode at around 310 nm when the Al composition in AlGaN multiple quantum wells (MQWs) exceeded 25% [9–11], due to the mixing of the topmost valence sub-bands. It is difficult to obtain a "normal" *c*-axis emission (vertical emission) from AlN (0001) or a high-Al-content AlGaN surface. So far, the LEE of ultraviolet radiation b (UVB) and UVC LEDs is very low (8%–10%) [12]. The LEE of the TM mode is weaker than that of the TE mode because the lateral travelling TM-mode photons cannot be easily extracted from the light escape cone [13]. Besides that, there are other underlying causes. For example, the p-GaN contact layer heavily absorbs UVC emissions, but switching to transparent p-AlGaN severely increases the forward voltage [1]. In order to improve the LEE of the UVC LED, various solutions have been proposed. LED chips were fabricated by substrate thinning [14] and hybrid photonic nanostructures [15]. Some have reported the overall enhancement of LEE and did not differentiate the TE and TM modes. Different kinds of substrate have been patterned, such as a sapphire substrate with a moth-eye pattern [16] and an AlN substrate with a roughened surface or sidewall roughening [17]. Some have reported a small enhancement in LEE of the TE mode but negligible LEE improvement in the TM mode.

In principle, as long as the TM-mode photon can be extracted out of the chip, the vertical emitted light output power can be greatly improved. The lateral emitted TM photon can be reflected or scattered by highly reflective omnidirectional reflectors [18], inclined sidewalls [19], and subwavelength grating [20] in the vertical direction. However, an effective methodology to improve the LEE of the TM mode has not been established so far to our knowledge. Here we propose a method to simultaneously improve both TE and especially TM emission, which can be applied to almost all commercially grown UVC LEDs without special epi-engineering or chip shaping.

2. EXPERIMENTAL DETAILS

The UV-LED epitaxial layer was grown on *c*-plane sapphire using the metal organic vapor phase epitaxy (MOVPE) method. From top to bottom, the epistructure consists of 200 nm p-GaN, a 30 nm p-AlGaN EBL, five pairs of 3 nm $Al_{0.42}Ga_{0.58}N$/3 nm $Al_{0.54}Ga_{0.46}N$ MQWs, 2 μm n-$Al_{0.6}Ga_{0.4}N$ with normal Si doping of 1×10^{19} cm^{-3}, a 1 μm AlN supperlattice (SL) layer, and a 1 μm undoped AlN buffer layer. After MOVPE growth, the samples were annealed in nitrogen ambient in order to activate the p-type conductivity. A regularly array of via holes with a pitch of 80–100 μm was formed through a laser scribing process. A 355 nm excimer laser with a repetition of 50 Hz was used, and the pulse energy was controlled at about 2 mJ/pulse, which makes the via hole extend from the p-GaN surface to the n-AlGaN layer. The via hole ensured the corrosive solution reached the n-AlGaN layer to initiate the electrochemical (EC) etching. Then the n-AlGaN layer was transformed into porous film by selective EC etching. EC etching was performed in a two-electrode cell at room temperature (RT) with Pt as the cathode. A 5 mm × 10 mm rectangular-shaped sample formed the anode, and a 98% HNO_3 solution was used as the electrolyte. The sample was slowly immersed in the HNO_3 solution using a dip coater. Constant voltage was supplied by Agilent B2900, and the EC etching was initiated. The EC etching of GaN was relatively easy and has been previously reported [21]. It is very difficult to make a regular doped AlGaN layer porous [22]. Therefore, a much higher voltage than that of n-GaN was applied. Several samples were etched at different external bias voltages from 20 to 120 V. Then 250 μm × 580 μm mesa structures were defined by inductively coupled plasma etching in order to expose the n-AlGaN surface. A Ni/Au p contact and a V/Al/V/Au n contact were deposited to form the p electrode and the n electrode, respectively. RT photoluminescence (PL) spectroscopy was carried out with a 500 cm spectrometer (2400 lines/mm grating). The spectral resolution of the instrument was 0.02 nm. The excitation source was a 248 nm KrF excimer laser with pulse frequency of 10 Hz, energy of 3.5 mJ, and pulse width of 10 ns. The laser spot size on the sample was limited to 3 mm × 3 mm by a slit. The angular-dependent PL was measured by a homemade angle-resolved system: the optical fiber rotated around the sample at a distance of 5 cm, and the PL was directly fed into the spectrometer. For the angular-dependent polarization measurement, a Glan–Taylor prism was inserted between the sample and the spectrometer. UV lenses were placed at both ends of a sleeve, and Glan–Taylor prisms were placed between the lenses. The sleeve was rotated around the *z* axis to measure far-field distribution. In the meantime, the polarizer was rotated to resolve the two electric fields that were perpendicular to the path of the light. The Raman spectrum was measured with a micro-confocal laser Raman spectrometer with spot size of 6 μm and spectral resolution of 0.2 cm^{-1}.

3. RESULTS AND DISCUSSION

The porous epilayer structure is shown in Fig. 1(a). The cross-sectional scanning electron microscope (SEM) image after via hole formation and EC etching at 40 V is shown in Fig. 1(b). The sample reveals the presence of uniform pores with a grating-like morphology. Figure 1(c) shows a bird's-eye view of the enlarged grating structures embedded in the n-AlGaN layers, the direction of which indicates the direction of EC etching. This characteristic is similar to the subwavelength grating. The grating spacing is about 90 nm, and the grating strip (the remaining n-AlGaN material) width is 10 nm.

The morphology of the nanoporous region can be controlled by anode bias. The pore size increases with the bias voltage. The average pore size is about 20 nm at 20 V and 240 nm at 120 V. Thus, the grating width decreases with increased voltage, but no obvious change of the grating spacing was observed. As a result, the largest voltage yields an almost completely removed sacrificial layer. The etched area shows different contrast from the unetched area and can be easily identified under the optical microscope. The etch process duration can be measured from the etching current versus time curve. Then the etching rate, calculated as the lateral etching depth divided by the etching time, was estimated as 1.67, 2.47, 3.84, and 4.16 μm/min under 30, 60, 80, and 120 V, respectively. It initially followed a linear relationship with the voltage and seemed to saturate at a high voltage. Figure 2(a) shows the RT PL for the unetched sample and four other etched samples. Figure 2(b) shows the linear relationship between the average size of the pore and the bias voltage. The laser absorption difference in the active region introduced by different pore sizes was corrected using a finite-difference time-domain (FDTD) simulation (not shown). The corrected PL enhancement ratio was calculated by comparing the PL intensity of the etched samples to the reference sample. In the range of 30–120 V, the enhancement rate of the PL is calculated to be from 16.3% to 61.7%. The average pore size shows a linear relationship with the PL

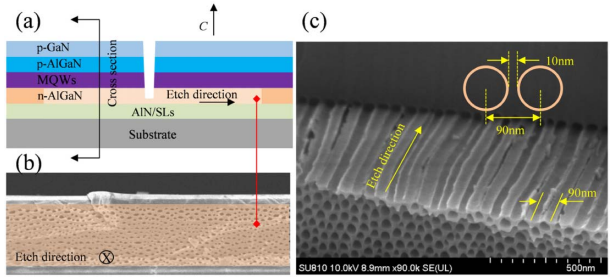

Fig. 1. (a) Epitaxial structure of the scribed via holes and porous layer. (b) Cross-sectional view of the nanoporous n-AlGaN layer etched at 40 V. (c) SEM image of the cleaved region in the porous layer showing the subwavelength grating structure at higher magnification.

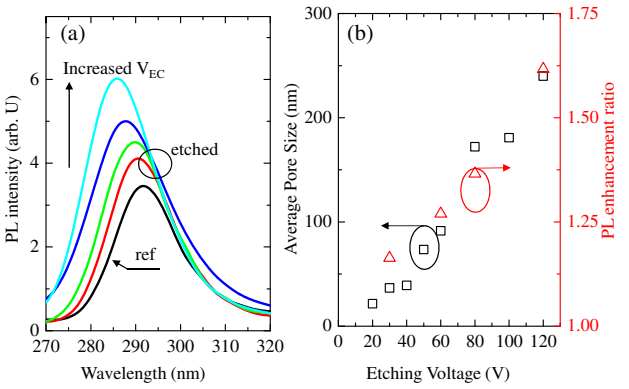

Fig. 2. (a) PL spectra of samples with different EC etching voltages. (b) Corrected PL enhancement ratio and average size of pore versus EC etching voltage.

intensity. The subwavelength grating structure induces strong diffraction of the guided modes and results in relatively high extraction efficiencies. The irregular shape of the nanopores increases the possibility of light being scattered and reflected upwards [23]. Due to such random scattering, the total internal reflection (TIR) is further reduced. The reabsorption loss from the MQWs and p-GaN decreased, and more photons were converted from the waveguide modes to the air modes. On the other hand, although the 6.1 eV band gap of AlN suggests that it should not be absorptive to photons with wavelengths longer than 205 nm, the 290 nm photons from the active region could well be absorbed due to the point defect.

The PL peak wavelength at different etching voltages is plotted in Fig. 3(b). Compared to the reference sample, the PL of the etched samples shows a blue-shift for 16.1, 27.9, 54.7, and 78.7 meV. The internal electric field modifies the electron and hole confinement potentials, resulting in reduced optical transition energy. Therefore, the large blue-shift of the PL peak implies the possibility of stress relaxation and reduction of the quantum-confined Stark effect (QCSE). This phenomenon can be explained by the strain modification caused by the deformation of the n-AlGaN epilayer. The strain state of the n-AlGaN layer was studied by Raman scattering. Figure 3(a) shows the Raman spectra of the etched and reference samples measured at RT with a backscattering configuration. Concerning the layer thickness, n-AlGaN with large thickness contributes to the broadening of Raman spectroscopy. The phonon mode near 597.2 cm^{-1} corresponds to the E_2^H (GaN-like) mode, while the photon mode near 659.25cm^{-1} corresponds to the E_2^H (AlN-like) mode, which confirms 60% of Al composition in n-AlGaN as designed [24,25]. The movement of E_2^H is a good indication of the stress state of the film. Figure 3(b) depicts the Raman shift of the E_2^H mode as a function of the etching voltage. A red-shift of the Raman peak from 597.2 cm^{-1} for the reference sample to 585.9 cm^{-1} for the sample etched at 120 V indicates that the compressive stress is largely released from the as-grown n-AlGaN to the porous n-AlGaN. Similar shifts have been reported in porous GaN and AlGaN previously [26,27]. The blue-shift of the PL peak position and the red-shift of Raman shift peak both indicate a decrease of compressive stress, and they lead to enhanced emission intensity [28–30].

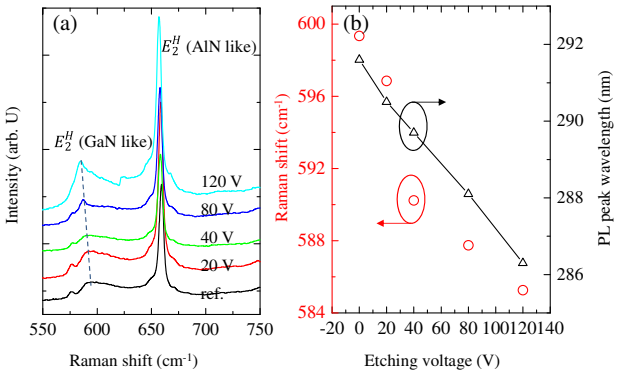

Fig. 3. (a) Raman spectra of the etched samples and the reference sample measured at RT. (b) Raman shift (left) and PL peak wavelength (right) as a function of etching voltages.

The measurement setup shown in Fig. 4(a) is used to test the angular-dependent far-field PL distribution as well as the PL polarization. At first, no lens or polarizer was placed in the light

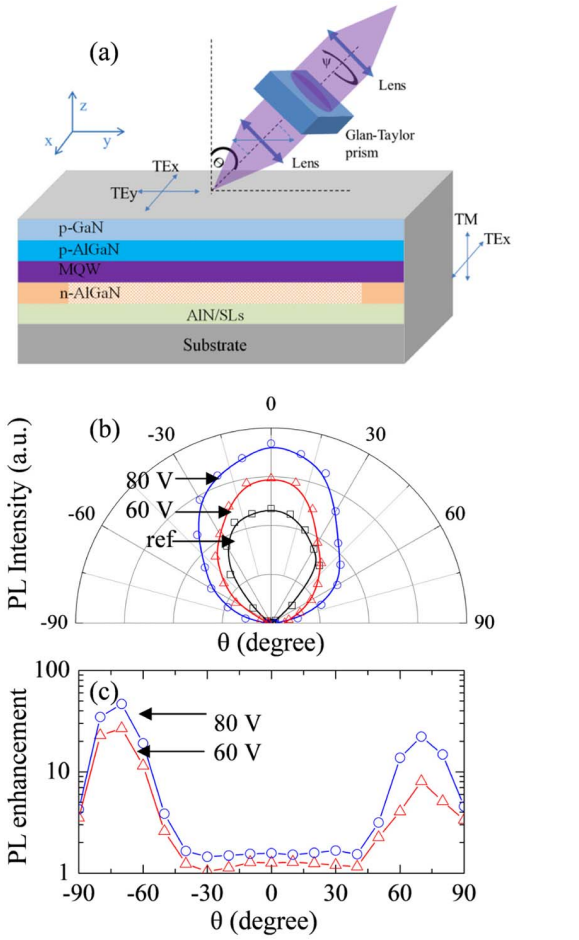

Fig. 4. (a) Schematic diagram of the angular-dependent polarization PL measurement. (b) Far-field PL distribution in polar coordinates. (c) Enhancement ratio of samples etched at 60 V and 80 V as a function of θ.

collection path, and thus the TE and TM modes were not differentiated. The detection orientation is parameterized by emission angle θ, which is the angle between the collection path and the c axis. The angular-dependent far-field PL distribution of the samples with and without a porous layer is shown in Fig. 4(b). The far-field distribution of the unetched reference sample is close to the Lambertian pattern, and the lateral emission is very weak ($\theta \sim \pm 90°$). The PL intensity of the etched sample was improved differently depending on the viewing angle θ. Samples etched at 60 V and 80 V show an enhancement factor of 1.27 and 1.57, respectively, in the vertical direction ($\theta = 0°$). In the lateral emission direction ($\theta \sim \pm 70°$), the enhancement factor is 8.1 for a 60 V etched sample and 22.2 for a 80 V etched sample [Fig. 4(c)]. The PL intensity and enhancement factor are not quite symmetric on both sides of the coordinates due to the irregular shape of the LED, and the above enhancement factor calculation gives the lower limit. The emission is no longer a Lambertian pattern because the lateral emission was enhanced by a much larger factor than the vertical emission, which means that the TE- and TM-mode emissions were improved at different ratios.

To figure out the different enhancement effects on TE- and TM-mode light, the polarization-dependent PL was collected at different emission angles θ. Both the TE mode and the TM mode were collected and can be measured individually by rotating the Glan-laser prism. ψ was the rotation angle of the polarizer's translucent shaft. At $\psi = 0°$, only the TE mode is collected at $\theta = 0°$, and the TM mode is collected at $\theta = \pm 90°$. By rotating the Glan–Taylor prism around the light emission direction, the intensity of electric field along the x axis $I_\perp$ and that of electric field in the y–z plane $I_\parallel$ can be resolved. The corresponding strength of $I_\perp$ and $I_\parallel$ can be expressed as

$$I_\parallel = I_{\mathrm{TE}y} \sin^2\theta + I_{\mathrm{TM}} \cos^2\theta, \quad (1)$$

$$I_\perp = I_{\mathrm{TE}x}, \quad (2)$$

where I_{TM} is the intensity of TM polarization in the z direction and $I_{\mathrm{TE}x}$, $I_{\mathrm{TE}y}$ are the intensity of TE polarization in x and y directions, respectively. The degree of polarization (DOP) was further calculated as

$$\mathrm{DOP} = (\mathrm{TE}_{\mathrm{total}} - \mathrm{TM}_{\mathrm{total}})/(\mathrm{TE}_{\mathrm{total}} + \mathrm{TM}_{\mathrm{total}}), \quad (3)$$

where $\mathrm{TE}_{\mathrm{total}}$ and $\mathrm{TM}_{\mathrm{total}}$ are integrated optical intensities and were calculated as

$$\mathrm{TE}_{\mathrm{total}} = I_{\mathrm{TE}y} \cos^2\theta + I_{\mathrm{TE}x}, \quad (4)$$

$$\mathrm{TM}_{\mathrm{total}} = I_{\mathrm{TM}} \sin^2\theta. \quad (5)$$

The angular distributions of the TE and TM modes are shown in Figs. 5(a) and 5(b), respectively. The emission pattern of TM-mode light, which depends on $\sin^2\theta$, is close to the results of previous reports [8,31,32]. After EC etching at 80 V, TE light increased 1.38 and 1.30 times at $\theta = 0°$ and $\theta = 60°$, respectively. For TM light, the enhancement factor can be ignored at $\theta = 0°$, and it increased 16.74 times at $\theta = 60°$. The enhanced TM mode shows a ribbon shape with maximum intensity at $\theta = 60°$. Such an enhanced ribbon shape indicates more TM-mode photons that travel laterally were extracted by the porous layer. In the reference sample, a large amount of UVC light is reabsorbed by the p-GaN layer as well as the active layer when it travels laterally and goes through a lot of TIR before emitting out of the device. The porous layer introduced more random scattering, which breaks the TIR, and the TM photon gets a greater chance of being extracted. It seems that the TM mode becomes more enhanced in lateral emission, while the TE mode becomes enhanced better in vertical emission. In principle, one could expect isotropic homogeneity at vertical emission and no difference between TE_x and TE_y. Therefore, rotating the Glan–Taylor prism does not change the spectrum much (not shown) for both the reference and etched samples at $\theta = 0°$. However, the results are quite different for side emission at $\theta = 60°$. The side emission for the reference unetched sample does not show particular polarization: the magnitude of TE_y is almost the same as that of TM, corresponding to a DOP of –0.08, which is close to the reported value [9,33,34]. For the 80 V etched sample, the TE mode increased by 13.51 times and the TM mode increased by 16.35 times [Fig. 5(c)]. Figure 5(d) shows the normalized PL intensity of the edge-emitting light with respect to the rotation angles ψ of the Glan-laser prism. It shows that the TM mode has a higher enhancement than TE_y and introduces a polarization (DOP = –0.242) for lateral emission [35]. The polarization switch from TE to TM depends on the strain of the quantum wells (QWs). It has been reported that for the same Al content, the polarization goes from TE- to TM-dominated emission by decreasing the compressive strain [36]. The reduction of compressive strain enhances the TM mode.

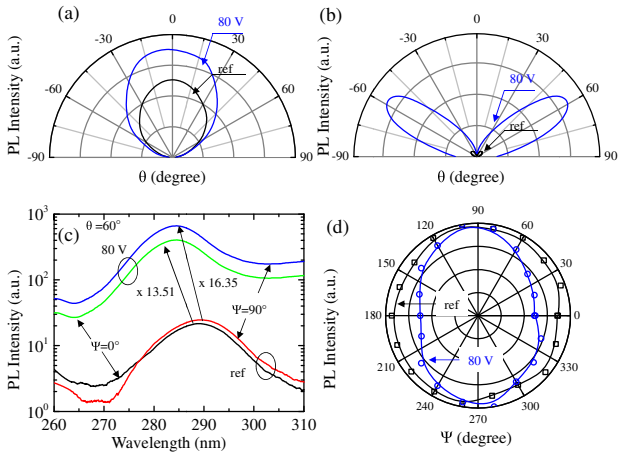

Fig. 5. Angular-dependent PL intensity profile in the (a) TE and (b) TM mode; (c) the side-emitting PL spectra at different polarization angles: $\psi = 0°$, $\psi = 90°$, when $\theta = 60°$; (d) the integrated PL intensity against polarization angle $\psi = 0°$–$360°$ of the reference unetched sample and 80 V etched sample, respectively.

Figure 6(a) shows the top-emitting electroluminescence (EL) spectra from 10 to 100 mA of the reference sample and the 80 V etched sample. For the reference sample, the QWs' peak is 289.89 nm at 10 mA and 292.92 nm at 100 mA. For the etched sample, the emission peak is 289.75 nm at 10 mA and 290.43 nm at 100 mA. The peak wavelength difference between the two samples is 2.49 nm (36.3 meV) at 100 mA, which is smaller than the shift observed in PL. Two weak shoulder peaks were found in both samples: 326.83, 357.37 nm in reference

sample and 329.08, 361.85 nm in the etched sample. It seems that they were not introduced by the porosification process. Similar secondary peaks from 320 to 330 nm were reported and were mostly likely related to overflow of the electron and its recombination in the p-AlGaN layer [5,37]. We attributed the parasitic peak around 360 nm to deep level defects introduced during the crystal growth [38,39]. Both emission windows can be eliminated in future studies by further optimization of the EBL and the number of MQWs to suppress the electron overflow. At 100 mA, the EL peak intensity enhancement is 15.2%, 22.7%, 32.5%, and 36.5% for samples etched at 20, 40, 60, and 80 V, respectively. At even higher etching voltage and with larger pores, the EL intensity of the samples did not increase significantly, and the electrical characteristics degraded gradually. This may be due to the destruction of the active region by severe EC etching. Figures 6(c) and 6(d) calculate the relative EQE curves of the 80 V etched sample and the reference sample, respectively. The EQE of both samples decreased with the increase of the injection current (efficiency droop). The efficiency droop range, defined as a percentage of the efficiency reduction at 100 mA with respect to its maximum level, was measured as 61% and 36% for the reference and the 80 V etched samples, respectively. There may be several reasons. The polarization-related effects may be a key factor for the efficiency droop in InGaN/GaN MQWs LEDs. Due to the existence of QCSE, the electron and hole wave functions are partially separated, resulting in the reduction of radiative recombination. The introduction of the porous layer promotes relaxation, reduces the band bending, and leads to the increase of the overlap of the electron and hole wave functions and thus reduces the radiation-free auger composite channel. The nonradiative recombination is also inhibited by the strain release process, resulting in the increase of light output power. The self-absorption of light in LEDs will produce heat, and the performance of the LEDs will deteriorate. Less self-absorption by the p-GaN layer as well as the active region resulting from the higher LEE of both the TE and TM modes may also contribute to the droop reduction at high injection current [40]. In addition, we believe that etching through the dislocation cores and surface-related traps also leads to EL enhancement. The voltage at 100 mA was measured as 16.2 V and 14.2 V for the sample etched at 80 V and the reference sample, respectively. Such number can be further reduced upon optimization of the electrode deposition and current spreading. The forward voltage of the etched sample is a little bit higher than that of the reference, and we attribute that to the degradation of the n-AlGaN conductivity.

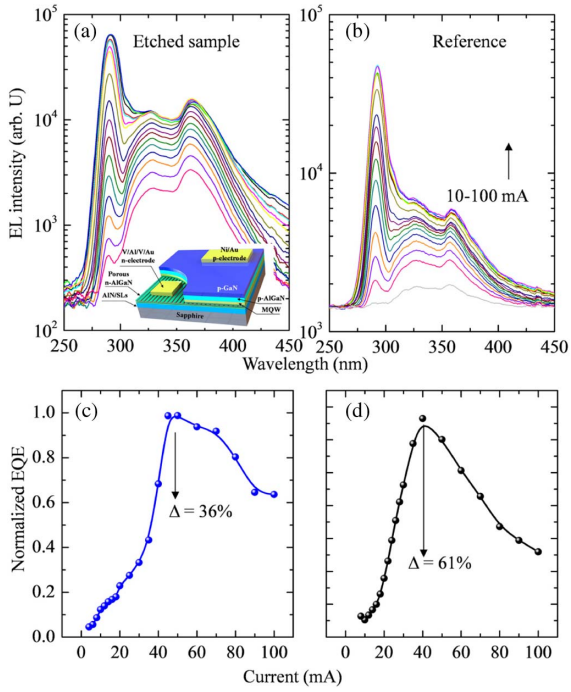

Fig. 6. EL spectra and normalized EQE versus current of (a), (c) the 80 V etched sample compared to (b), (d) the reference sample. The inset of (a) shows the schematic of the porous LED.

4. CONCLUSIONS

In conclusion, we used EC etching to prepare a nanoporous n-AlGaN layer in the regular grown 290 nm UV LED. The TM mode has a much larger enhancement factor compared to the TE mode. It results in 1.57 and 22 times intensity improvement for the top and side PL emission, respectively. The random scattering by the nanoporous layer is helpful to decrease the TIR and reabsorption of emitted photons by the p-GaN layer and the active region, which especially benefits the TM-mode photons to escape. The compressive strain relaxation introduced by the nanoporous layer was verified by Raman measurement and PL wavelength shift. The strain relaxation is helpful to inhibit the occurrences of nonradiative recombination and reduce the QCSE effect. All these effects contribute to the 36.5% improved light output power and reduction of the EQE droop from 61% to 36% at 100 mA. These results indicate that the nanoporous n-AlGaN layer is a promising method to achieve high-efficiency UVC LEDs.

Funding. National Natural Science Foundation of China (61574114, 61774121); National Key Research and Development Program of China (2016YFB0400801); Fundamental Research Funds for the Central Universities (Z201805198).

Disclosures. The authors declare that there are no conflicts of interest related to this paper.

REFERENCES

1. H. Hirayama, N. Maeda, S. Fujikawa, S. Toyoda, and N. Kamata, "Recent progress and future prospects of AlGaN-based high-efficiency deep-ultraviolet light-emitting diodes," Jpn. J. Appl. Phys. **53**, 100209 (2014).
2. T. Takano, T. Mino, J. Sakai, N. Noguchi, K. Tsubaki, and H. Hirayama, "Deep-ultraviolet light-emitting diodes with external quantum efficiency higher than 20% at 275 nm achieved by improving light-extraction efficiency," Appl. Phys. Express **10**, 031002 (2017).
3. Y. Nagasawa and A. Hirano, "A review of AlGaN-based deep-ultraviolet light-emitting diodes on sapphire," Appl. Sci. **8**, 1264 (2018).
4. J. Brodrick, M. Pattison, N. Bardsley, C. Elliot, M. Hansen, K. Lee, L. Pattison, J. Tsao, and M. Yamada, "2018 Solid-State Lighting R&D Opportunities," DOE BTO SSL Program, DOE/EE-1907, https://www.energy.gov/sites/prod/files/2019/02/f59/edit.ssl_rd-opportunities_jan2019.pdf (2019).

5. S. Tan, J. Zhang, T. Egawa, and G. Chen, "Influence of quantum-well number and an AlN electron blocking layer on the electroluminescence properties of AlGaN deep ultraviolet light-emitting diodes," Appl. Sci. **8**, 2402 (2018).
6. N. Susilo, S. Hagedorn, D. Jaeger, H. Miyake, U. Zeimer, C. Reich, B. Neuschulz, L. Sulmoni, M. Guttmann, F. Mehnke, C. Kuhn, T. Wernicke, M. Weyers, and M. Kneissl, "AlGaN-based deep UV LEDs grown on sputtered and high temperature annealed AlN/sapphire," Appl. Phys. Lett. **112**, 041110 (2018).
7. B. T. Tran, N. Maeda, M. Jo, D. Inoue, T. Kikitsu, and H. Hirayama, "Performance improvement of AlN crystal quality grown on patterned Si(111) substrate for deep UV-LED applications," Sci. Rep. **6**, 35681 (2016).
8. H.-Y. Ryu, I.-G. Choi, H.-S. Choi, and J.-I. Shim, "Investigation of light extraction efficiency in AlGaN deep-ultraviolet light-emitting diodes," Appl. Phys. Express **6**, 062101 (2013).
9. T. Kolbe, A. Knauer, C. Chua, Z. Yang, S. Einfeldt, P. Vogt, N. M. Johnson, M. Weyers, and M. Kneissl, "Optical polarization characteristics of ultraviolet (In)(Al)GaN multiple quantum well light emitting diodes," Appl. Phys. Lett. **97**, 171105 (2010).
10. M. Hou, Z. Qin, C. He, J. Cai, X. Wang, and B. Shen, "Effect of injection current on the optical polarization of AlGaN-based ultraviolet light-emitting diodes," Opt. Express **22**, 19589–19594 (2014).
11. M. F. Schubert, S. Chhajed, J. K. Kim, E. F. Schubert, and J. Cho, "Polarization of light emission by 460 nm GaInN/GaN light-emitting diodes grown on (0001) oriented sapphire substrates," Appl. Phys. Lett. **91**, 051117 (2007).
12. H. Hirayama, S. Fujikawa, N. Noguchi, J. Norimatsu, T. Takano, K. Tsubaki, and N. Kamata, "222–282 nm AlGaN and InAlGaN-based deep-UV LEDs fabricated on high-quality AlN on sapphire," Phys. Status Solidi A **206**, 1176–1182 (2009).
13. K. B. Nam, J. Li, M. L. Nakarmi, J. Y. Lin, and H. X. Jiang, "Unique optical properties of AlGaN alloys and related ultraviolet emitters," Appl. Phys. Lett. **84**, 5264–5266 (2004).
14. J. R. Grandusky, J. Chen, S. R. Gibb, M. C. Mendrick, C. G. Moe, L. Rodak, G. A. Garrett, M. Wraback, and L. J. Schowalter, "270 nm pseudomorphic ultraviolet light-emitting diodes with over 60 mW continuous wave output power," Appl. Phys. Express **6**, 032101 (2013).
15. S. Inoue, Naoki, and M. Taniguchi, "150 mW deep-ultraviolet light-emitting diodes with large-area AlN nanophotonic light-extraction structure emitting at 265 nm," Appl. Phys. Lett. **110**, 141106 (2017).
16. S. Wang, J. Dai, J. Hu, S. Zhang, L. Xu, H. Long, J. Chen, Q. Wan, H.-C. Kuo, and C. Chen, "Ultrahigh degree of optical polarization above 80% in AlGaN-based deep-ultraviolet LED with moth-eye microstructure," ACS Photon. **5**, 3534–3540 (2018).
17. Y. Guo, Y. Zhang, J. Yan, H. Xie, L. Liu, X. Chen, M. Hou, Z. Qin, J. Wang, and J. Li, "Light extraction enhancement of AlGaN-based ultraviolet light-emitting diodes by substrate sidewall roughening," Appl. Phys. Lett. **111**, 011102 (2017).
18. J. W. Lee, J. H. Park, D. Y. Kim, E. F. Schubert, J. Kim, J. Lee, Y.-I. Kim, Y. Park, and J. K. Kim, "Arrays of truncated cone AlGaN deep-ultraviolet light-emitting diodes facilitating efficient outcoupling of in-plane emission," ACS Photon. **3**, 2030–2034 (2016).
19. Y. Zhang, R. Meng, Z.-H. Zhang, Q. Shi, L. Li, G. Liu, and W. Bi, "Effects of inclined sidewall structure with bottom metal air cavity on the light extraction efficiency for AlGaN-based deep ultraviolet light-emitting diodes," IEEE Photon. J. **9**, 1600709 (2017).
20. Y. Takashima, R. Shimizu, M. Haraguchi, and Y. Naoi, "Polarized emission characteristics of UV-LED with subwavelength grating," Jpn. J. Appl. Phys. **53**, 072101 (2014).
21. G. Yuan, K. Xiong, C. Zhang, Y. Li, and J. Han, "Optical engineering of modal gain in a III-nitride laser with nanoporous GaN," ACS Photon. **3**, 1604–1610 (2016).
22. T. Detchprohm, Y.-S. Liu, K. Mehta, S. Wang, H. Xie, T.-T. Kao, S.-C. Shen, P. D. Yoder, F. A. Ponce, and R. D. Dupuis, "Sub 250 nm deep-UV AlGaN/AlN distributed Bragg reflectors," Appl. Phys. Lett. **110**, 011105 (2017).
23. J. J. Wierer, A. A. Allerman, I. Montano, and M. W. Moseley, "Influence of optical polarization on the improvement of light extraction efficiency from reflective scattering structures in AlGaN ultraviolet light-emitting diodes," Appl. Phys. Lett. **105**, 061106 (2014).
24. A. Najar, M. Gerland, and M. Jouiad, "Porosity-induced relaxation of strains in GaN layers studied by means of micro-indentation and optical spectroscopy," J. Appl. Phys. **111**, 093513 (2012).
25. V. Y. Davydov, I. N. Goncharuk, A. N. Smirnov, A. E. Nikolaev, W. V. Lundin, A. S. Usikov, A. A. Klochikhin, J. Aderhold, J. Graul, O. Semchinova, and H. Harima, "Composition dependence of optical phonon energies and Raman line broadening in hexagonal $Al_xGa_{1-x}N$ alloys," Phys. Rev. B **65**, 125203 (2002).
26. H. Hartono, C. B. Soh, S. Y. Chow, S. J. Chua, and E. A. Fitzgerald, "Reduction of threading dislocation density in GaN grown on strain relaxed nanoporous GaN template," Appl. Phys. Lett. **90**, 171917 (2007).
27. L. Zhang, Y. N. Guo, J. C. Yan, Q. Q. Wu, X. C. Wei, J. X. Wang, and J. M. Li, "Deep ultraviolet light-emitting diodes with improved performance via nanoporous AlGaN template," Opt. Express **27**, 4917–4926 (2019).
28. S.-J. Kim, K. J. Lee, S. Oh, J.-H. Han, D. S. Lee, and S.-J. Park, "Enhanced performance of InGaN/GaN MQW LED with strain-relaxing Ga-doped ZnO transparent conducting layer," Opt. Express **27**, A458–A467 (2019).
29. T. Y. Wang, C. T. Tasi, C. F. Lin, and D. S. Wuu, "85% internal quantum efficiency of 280-nm AlGaN multiple quantum wells by defect engineering," Sci. Rep. **7**, 14422 (2017).
30. H. Hu, S. Zhou, H. Wan, X. Liu, N. Li, and H. Xu, "Effect of strain relaxation on performance of InGaN/GaN green LEDs grown on 4-inch sapphire substrate with sputtered AlN nucleation layer," Sci. Rep. **9**, 3447 (2019).
31. Y. Taniyasu and M. Kasu, "Surface 210 nm light emission from an AlN p-n junction light-emitting diode enhanced by A-plane growth orientation," Appl. Phys. Lett. **96**, 221110 (2010).
32. X. Chen, C. Ji, Y. Xiang, X. Kang, B. Shen, and T. Yu, "Angular distribution of polarized light and its effect on light extraction efficiency in AlGaN deep-ultraviolet light-emitting diodes," Opt. Express **24**, A935–A942 (2016).
33. J.-I. Chyi, M.-H. Lo, Y. Nanishi, Y.-J. Cheng, H.-C. Kuo, H. Morkoç, J. Piprek, S.-C. Wang, and E. Yoon, "Fabrication and lasing characteristics of GaN nanopillars," Proc. SPIE **7939**, 79391T (2011).
34. J. E. Northrup, C. L. Chua, Z. Yang, T. Wunderer, M. Kneissl, N. M. Johnson, and T. Kolbe, "Effect of strain and barrier composition on the polarization of light emission from AlGaN/AlN quantum wells," Appl. Phys. Lett. **100**, 021101 (2012).
35. C. Liu, Y. K. Ooi, S. M. Islam, H. Xing, D. Jena, and J. Zhang, "234 nm and 246 nm AlN-Delta-GaN quantum well deep ultraviolet light-emitting diodes," Appl. Phys. Lett. **112**, 011101 (2018).
36. Z. Bryan, I. Bryan, S. Mita, J. Tweedie, Z. Sitar, and R. Collazo, "Strain dependence on polarization properties of AlGaN and AlGaN-based ultraviolet lasers grown on AlN substrates," Appl. Phys. Lett. **106**, 232101 (2015).
37. J. Yan, J. Wang, Y. Zhang, P. Cong, L. Sun, Y. Tian, C. Zhao, and J. Li, "AlGaN-based deep-ultraviolet light-emitting diodes grown on High-quality AlN template using MOVPE," J. Cryst. Growth **414**, 254–257 (2015).
38. M. Shatalov, W. Sun, A. Lunev, X. Hu, A. Dobrinsky, Y. Bilenko, J. Yang, M. Shur, R. Gaska, C. Moe, G. Garrett, and M. Wraback, "AlGaN deep-ultraviolet light-emitting diodes with external quantum efficiency above 10%," Appl. Phys. Express **5**, 082101 (2012).
39. C. De Santi, M. Meneghini, D. Monti, J. Glaab, M. Guttmann, J. Rass, S. Einfeldt, F. Mehnke, J. Enslin, T. Wernicke, M. Kneissl, G. Meneghesso, and E. Zanoni, "Recombination mechanisms and thermal droop in AlGaN-based UV-B LEDs," Photon. Res. **5**, A44–A51 (2017).
40. P.-M. Tu, J.-R. Chang, S.-C. Huang, S.-K. Yang, Y.-W. Lin, T.-C. Hung, C.-P. Hsu, and C.-Y. Chang, "Investigation of efficiency droop for UV LED with N-type AlGaN layer," Proc. SPIE **8278**, 82781B (2012).